

A New Method for Determining the Leakage Inductances of a Nine-Phase Synchronous Machine from No-Load and Short-Circuit Tests

Alberto Tassarolo, *IEEE Senior Member*, Sobhan Mohamadian and Mauro Bortolozzi

Abstract—The accurate determination of stator leakage inductances is presently an open issue in the analysis and testing of multiphase electric machines. Calculation methods are available which involve complicated and often poorly precise 3D analyses. Experimental determination techniques, using measurements on the wound stator with the rotor removed, are also possible but quite impractical as they need to be performed during machine manufacturing or require rotor withdrawal. In this paper, a new approach is proposed to determine all the stator self and mutual leakage inductances of a nine-phase synchronous machine based on a minimal set (a couple) of magneto-static finite element (FE) simulations and on the measurements taken during no-load and short circuit routine tests. The procedure is applied to a wound-field salient pole nine-phase synchronous generator for validation, showing a good accordance with the results obtained from measurements on the machine with the rotor removed. A discussion is also proposed on the possibility to extend the presented procedure to other multiphase topologies.

Index Terms—nine-phase machines, parameter identification, stator leakage inductances, synchronous machines, vector space decomposition.

I. INTRODUCTION

MULTI-PHASE synchronous machines are widely used today thanks to their well-known advantages over three-phase ones, in terms of performance, fault tolerance and flexibility of operation [1], [2]. In particular, an important multiphase machine design which is often taken into account is the nine-phase one. Example of nine-phase synchronous machines can be found in the field of power generation [3]-[5], permanent-magnet motor drives [6]-[8] and multi-motor applications [9].

In the analysis and testing of multiphase machines, a sufficiently accurate determination of their stator leakage inductances is still an open issue of some possible practical importance. Leakage inductances, in fact, can importantly impact on machine performance [10], especially in presence of time and space harmonics [11]-[14].

The problem of determining stator leakage inductances of electric machines from tests has been widely addressed in the technical literature. Experimental procedures are proposed for this purpose in [15] applying to three-phase induction motors based on impedance measurements on the machine with the rotor at stand-still. As regards three-phase synchronous machines, experimental methods are addressed in [16] to characterize their saturated dq model where the rotor is represented with a generic linear equivalent circuit [17]. Stator leakage inductances, together with the other dq

model parameters, are identified in [16] based on standstill frequency response (SSFR) measurements suitably processed through genetic algorithms. Finally, some experimental procedures can be found in the literature to measure the end-coil and slot leakage inductances of multiphase machines based on dedicated tests to be conducted on the wound stator with the rotor removed combined with suitably calibrated Finite Element Analysis (FEA) simulations [18]-[21].

This paper proposes a new alternative method to determine the overall stator leakage inductances of a nine-phase synchronous machine using the no-load and the short-circuit tests combined with a minimal set of FEA magneto-static simulations. The latter are used to identify magnetizing inductances as functions of the rotor position according to [22], which can be accomplished with only two magneto-static FEA simulations. The short circuit and no-load tests [18], on the other side, are used to record the no-load voltage and short-circuit current waveforms.

The basic idea of the proposed methodology is to derive the accurate mathematical model of the machine by identifying stator magnetizing inductances through FEA simulations as per [22] and treating leakage inductances as unknown parameters. On the machine model, transformed through the Vector Space Decomposition (VSD) technique [23], the condition is then imposed that the short circuit current waveform must equal the measured one when the rotor-produced back-emf equals the one recorded in the no-load test. This leads to a set of nonlinear algebraic equations from which the leakage inductances (unknowns) can be obtained. In the procedure, rotor circuit parameters are not involved and thereby do not need to be estimated or measured.

Compared to [16], the proposed technique employs measurements which can be taken during usual no-load and sustained short-circuit acceptance tests [18] and does not require any frequency response characterization or processing. Furthermore, the work in [16] is tailored on three-phase machines, while this paper necessarily addresses high-phase-order stator topologies as it exploits harmonic circulation currents which specifically occur in multiphase machines in sustained short-circuit conditions or under Voltage-Source Inverter (VSI) supply as discussed in [11], [12], [22]. On the other side, unlike the tests with the rotor removed [18]-[21], the presented approach does not require rotor withdrawal and can be therefore implemented on the built machine and not in the manufacturing stage.

The method described in this paper is applied to the computation of the leakage inductances of a nine-phase salient-pole synchronous machine prototype. The results are compared to those obtained with more traditional approaches based on measurements on the machine with the rotor removed [18]-[21], showing a good accordance. The

Alberto Tassarolo and Mauro Bortolozzi are with the Engineering and Architecture Department of the University of Trieste, Trieste, Italy (email: atessarolo@units.it, mauro.bortolozzi@phd.units.it).

Sobhan Mohamadian is with the Electrical Engineering Department of Iran University of Science and Technology, Tehran, Iran (email: s_mohamadian@iust.ac.ir).

same experimental validation is repeated twice on the same machine equipped with two different rotors having identical geometry, but one with and the other without damper circuits. The tests with the two different rotors are shown to give practically the same results. This confirms that the proposed methodology is not affected by the presence of rotor circuits and does not require their characterization.

The paper is organized as follows. In Section II the nine-phase machine model is presented in both phase variables and after VSD transformation. In Section III the model is particularized to reproduce steady-state short-circuit conditions; in Section IV the algebraic equations are derived to identify stator leakage inductances from no-load and short-circuit test measurements. Section V describes the application of the procedure to a nine-phase machine prototype (with and without rotor damper cage). In Section VI the results are validated against the leakage inductance independently measurement [18] on the same machine with the rotor removed and a clarification is provided of why 2D FEA does not suffice, in general, for the purpose of an accurate estimation of leakage inductances. Finally, Section VII discusses the merits of the proposed approach and the possibility (presently under study) to extend it to other multiphase designs.

II. MACHINE MATHEMATICAL MODEL

The stator phases of a nine-phase machine are conventionally numbered from 0 to 8 and named as depicted in the diagrams shown in Fig. 1 according to the scheme proposed in [11], [23]. It can be seen that, based on this convention, two subsequent phases are displaced by $\pi/9$ electrical radians. Phase voltages, flux linkages, currents and rotor-produced back-emf's are indicated as $v_0 \dots v_8$, $\varphi_0 \dots \varphi_8$, $i_0 \dots i_8$, $e_0 \dots e_8$, respectively.

A. Machine model in phase variables

The mathematical model of a nine-phase machine, expressed in phase variables (subscript ph) is:

$$\mathbf{v}_{ph} = r_s \mathbf{i}_{ph} + \frac{d}{dt} \boldsymbol{\varphi}_{ph} + \mathbf{e}_{ph}, \quad (1)$$

where r_s is the phase resistance and

$$\mathbf{v}_{ph} = (v_0 \ v_1 \ \dots \ v_8)^t, \quad \boldsymbol{\varphi}_{ph} = (\varphi_0 \ \varphi_1 \ \dots \ \varphi_8)^t, \quad (2)$$

$$\mathbf{i}_{ph} = (i_0 \ i_1 \ \dots \ i_8)^t, \quad \mathbf{e}_{ph} = (e_0 \ e_1 \ \dots \ e_8)^t.$$

The flux linkage vector can be expressed as

$$\boldsymbol{\varphi}_{ph} = (\mathbf{L}_{ph} + \mathbf{M}_{ph}) \mathbf{i}_{ph} \quad (3)$$

where \mathbf{L}_{ph} , \mathbf{M}_{ph} are the leakage inductance and magnetizing inductance matrices, respectively. Under the assumption that leakage inductances do not vary with the rotor position [24], \mathbf{L}_{ph} takes the following form

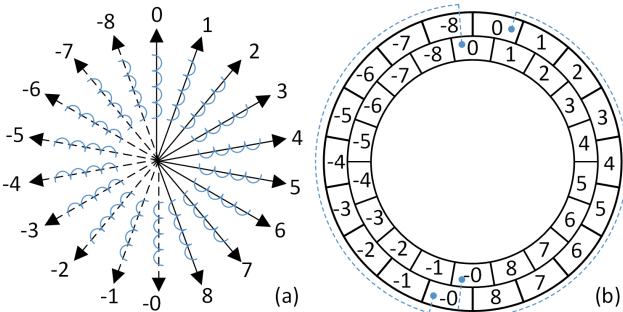


Fig. 1. Phase numbering and arrangement for a two-pole nine-phase machine in the form of: (a) vector diagram; (b) phase belt arrangement in a two-layer short-pitch winding. The dashed line exemplifies the end-winding connections for phase "0".

$$\mathbf{L}_{ph} = \begin{pmatrix} l_0 & l_1 & l_2 & l_3 & l_4 & -l_4 & -l_3 & -l_2 & -l_1 \\ l_1 & l_0 & l_1 & l_2 & l_3 & l_4 & -l_4 & -l_3 & -l_2 \\ l_2 & l_1 & l_0 & l_1 & l_2 & l_3 & l_4 & -l_4 & -l_3 \\ l_3 & l_2 & l_1 & l_0 & l_1 & l_2 & l_3 & l_4 & -l_4 \\ l_4 & l_3 & l_2 & l_1 & l_0 & l_1 & l_2 & l_3 & l_4 \\ -l_4 & l_4 & l_3 & l_2 & l_1 & l_0 & l_1 & l_2 & l_3 \\ -l_3 & -l_4 & l_4 & l_3 & l_2 & l_1 & l_0 & l_1 & l_2 \\ -l_2 & -l_3 & -l_4 & l_4 & l_3 & l_2 & l_1 & l_0 & l_1 \\ -l_1 & -l_2 & -l_3 & -l_4 & l_4 & l_3 & l_2 & l_1 & l_0 \end{pmatrix}, \quad (4)$$

where l_0 indicates the leakage self-inductance of a phase and l_j (with j standing for a generic integer number between 1 and 4) represents the mutual leakage inductance between two phases displaced by $j\frac{\pi}{9}$ electrical radians. The five independent inductances l_0, l_1, l_2, l_3, l_4 are the five unknown parameters which are to be identified.

The matrix \mathbf{M}_{ph} , on the other side, can be written as:

$$\mathbf{M}_{ph}(\theta) = \begin{pmatrix} m_{0,0}(\theta) & m_{0,1}(\theta) & \dots & m_{0,8}(\theta) \\ m_{1,0}(\theta) & m_{1,1}(\theta) & \dots & m_{1,8}(\theta) \\ \vdots & \vdots & \ddots & \vdots \\ m_{8,0}(\theta) & m_{8,1}(\theta) & \dots & m_{8,8}(\theta) \end{pmatrix} \quad (5)$$

where $m_{i,j}$ is the mutual inductance (due to the air-gap flux) between phases i and j ($i, j = 0, 1, \dots, 8$) and, in particular, $m_{j,j}$ indicates the self-inductance (due to the air-gap flux) of phase j . Such inductances depend on the rotor position in case of salient-pole machines and can be expressed as follows [22]:

$$m_{i,j}(\theta) = \frac{\pi R L \mu_0}{2} \left\{ \sum_{r,s=1,3,5,7,9} F_s W_r P_{s+r} \cos[(si+rj)\alpha - (s+r)\theta] + \sum_{\substack{r,s=1,3,5,7,9 \\ r \neq s}} F_s W_r P_{|s-r|} \cos[(si-rj)\alpha - (s-r)\theta] + \sum_{s=1,3,5,7,9} F_s W_s P_0 \cos[s(i-j)\alpha] \right\} \quad (6)$$

where R is the mean air-gap radius, $\alpha = \pi/9$ is the phase progression, L is the machine core length, μ_0 is the magnetic permeability of the air and F_s, W_r, P_k (with s, r, k being integer indices) are Fourier coefficients that can be found as explained in [22] from two magneto-static FEA simulations. In (6), the first nine odd space harmonics are considered for inclusion in the machine model, as they generally have the highest amplitude [24], [25] (V.A). More space harmonics cannot be included in the model because this would result in a time-varying inductance matrix after application of the VSD transform [24], [25] as discussed in the next section.

B. Machine model after VSD

The VSD is a particular transformation which enables to express the machine model in the form of a linear differential equation with time-invariant parameters [2]. For a nine-phase machine, the VSD can be achieved by defining the following real-valued 9×9 transformation matrices:

$$\mathbf{C} = \sqrt{\frac{2}{9}} \begin{pmatrix} 1 & \cos(\alpha) & \cos(2\alpha) & \cos(3\alpha) & \dots & \cos(8\alpha) \\ 0 & \sin(\alpha) & \sin(2\alpha) & \sin(3\alpha) & \dots & \sin(8\alpha) \\ 1 & \cos(3\alpha) & \cos(6\alpha) & \cos(9\alpha) & \dots & \cos(24\alpha) \\ 0 & \sin(3\alpha) & \sin(6\alpha) & \sin(9\alpha) & \dots & \sin(24\alpha) \\ 1 & \cos(5\alpha) & \cos(10\alpha) & \cos(15\alpha) & \dots & \cos(40\alpha) \\ 0 & \sin(5\alpha) & \sin(10\alpha) & \sin(15\alpha) & \dots & \sin(40\alpha) \\ 1 & \cos(7\alpha) & \cos(14\alpha) & \cos(21\alpha) & \dots & \cos(56\alpha) \\ 0 & \sin(7\alpha) & \sin(14\alpha) & \sin(21\alpha) & \dots & \sin(56\alpha) \\ \frac{1}{\sqrt{2}} & \frac{1}{\sqrt{2}} \cos(9\alpha) & \frac{1}{\sqrt{2}} \cos(18\alpha) & \frac{1}{\sqrt{2}} \cos(27\alpha) & \dots & \frac{1}{\sqrt{2}} \cos(72\alpha) \end{pmatrix} \quad (7)$$

$$\mathbf{P}(\theta) = \begin{pmatrix} \mathbf{P}_1(\theta) & \mathbf{0}_{2 \times 2} & \mathbf{0}_{2 \times 2} & \mathbf{0}_{2 \times 2} & \mathbf{0}_{2 \times 1} \\ \mathbf{0}_{2 \times 2} & \mathbf{P}_3(\theta) & \mathbf{0}_{2 \times 2} & \mathbf{0}_{2 \times 2} & \mathbf{0}_{2 \times 1} \\ \mathbf{0}_{2 \times 2} & \mathbf{0}_{2 \times 2} & \mathbf{P}_5(\theta) & \mathbf{0}_{2 \times 2} & \mathbf{0}_{2 \times 1} \\ \mathbf{0}_{2 \times 2} & \mathbf{0}_{2 \times 2} & \mathbf{0}_{2 \times 2} & \mathbf{P}_7(\theta) & \mathbf{0}_{2 \times 1} \\ \mathbf{0}_{1 \times 2} & \mathbf{0}_{1 \times 2} & \mathbf{0}_{1 \times 2} & \mathbf{0}_{1 \times 2} & 1 \end{pmatrix} \quad (8)$$

where $\mathbf{0}_{2 \times 2}$ is the 2×2 null matrix and

$$\mathbf{P}_h(\theta) = \begin{pmatrix} \cos(h\theta) & \sin(h\theta) \\ -\sin(h\theta) & \cos(h\theta) \end{pmatrix}, \quad \mathbf{0}_{2 \times 1} = \mathbf{0}_{1 \times 2}^t = \begin{pmatrix} 0 \\ 0 \end{pmatrix} \quad (9)$$

for any integer $h \in \{1, 3, 5, 7\}$.

The overall transformation matrix is defined as:

$$\mathbf{T}(\theta) = \mathbf{P}(\theta)\mathbf{C} \quad (10)$$

By a symbolic math tool it can be easily checked that the following identities hold for $\mathbf{T}(\theta)$:

$$\mathbf{T}(\theta)\mathbf{T}(\theta)^t = \mathbf{I}_9 \quad (11)$$

$$\mathbf{J} = \mathbf{T}(\theta) \left[\frac{d}{d\theta} \mathbf{T}(\theta)^t \right] = \begin{pmatrix} \mathbf{J}_2 & \mathbf{0}_{2 \times 2} & \mathbf{0}_{2 \times 2} & \mathbf{0}_{2 \times 2} & \mathbf{0}_{2 \times 1} \\ \mathbf{0}_{2 \times 2} & 3\mathbf{J}_2 & \mathbf{0}_{2 \times 2} & \mathbf{0}_{2 \times 2} & \mathbf{0}_{2 \times 1} \\ \mathbf{0}_{2 \times 2} & \mathbf{0}_{2 \times 2} & 5\mathbf{J}_2 & \mathbf{0}_{2 \times 2} & \mathbf{0}_{2 \times 1} \\ \mathbf{0}_{2 \times 2} & \mathbf{0}_{2 \times 2} & \mathbf{0}_{2 \times 2} & 7\mathbf{J}_2 & \mathbf{0}_{2 \times 1} \\ \mathbf{0}_{1 \times 2} & \mathbf{0}_{1 \times 2} & \mathbf{0}_{1 \times 2} & \mathbf{0}_{1 \times 2} & 0 \end{pmatrix} \quad (12)$$

where \mathbf{I}_9 is the 9×9 identity matrix and

$$\mathbf{J}_2 = \begin{pmatrix} 0 & -1 \\ 1 & 0 \end{pmatrix} \quad (13)$$

By applying $\mathbf{T}(\theta)$ to the phase variables (2) we obtain the transformed current, voltage, flux linkage and rotor-produced back-emf vector variables as follows:

$$\mathbf{v}_{vsd} = \mathbf{T}\mathbf{v}_{ph}, \quad \boldsymbol{\varphi}_{vsd} = \mathbf{T}\boldsymbol{\varphi}_{ph}, \quad \mathbf{i}_{vsd} = \mathbf{T}\mathbf{i}_{ph}, \quad \mathbf{e}_{vsd} = \mathbf{T}\mathbf{e}_{ph} \quad (14)$$

where

$$\mathbf{v}_{vsd} = (v_{d1} \ v_{q1} \ | \ v_{d3} \ v_{q3} \ | \ v_{d5} \ v_{q5} \ | \ v_{d7} \ v_{q7} \ | \ v_9)^t \quad (15)$$

$$\boldsymbol{\varphi}_{vsd} = (\varphi_{d1} \ \varphi_{q1} \ | \ \varphi_{d3} \ \varphi_{q3} \ | \ \varphi_{d5} \ \varphi_{q5} \ | \ \varphi_{d7} \ \varphi_{q7} \ | \ \varphi_9)^t \quad (16)$$

$$\mathbf{i}_{vsd} = (i_{d1} \ i_{q1} \ | \ i_{d3} \ i_{q3} \ | \ i_{d5} \ i_{q5} \ | \ i_{d7} \ i_{q7} \ | \ i_9)^t \quad (17)$$

$$\mathbf{e}_{vsd} = (e_{d1} \ e_{q1} \ | \ e_{d3} \ e_{q3} \ | \ e_{d5} \ e_{q5} \ | \ e_{d7} \ e_{q7} \ | \ e_9)^t \quad (18)$$

Matrices \mathbf{L}_{ph} , \mathbf{M}_{ph} are also transformed as follows:

$$\mathbf{L}_{vsd} = \mathbf{T}\mathbf{L}_{ph}\mathbf{T}^t, \quad \mathbf{M}_{vsd} = \mathbf{T}\mathbf{M}_{ph}\mathbf{T}^t \quad (19)$$

By left-multiplying both the members of (1) by \mathbf{T} and using (14), (19) together with the identities (10)-(12) we can finally write:

$$\mathbf{v}_{vsd} = r_s \mathbf{i}_{vsd} + \omega \mathbf{J} (\mathbf{L}_{vsd} + \mathbf{M}_{vsd}) \mathbf{i}_{vsd} + (\mathbf{L}_{vsd} + \mathbf{M}_{vsd}) \frac{d}{dt} \mathbf{i}_{vsd} + \mathbf{e}_{vsd} \quad (20)$$

which is the sought differential equation representing the machine constant-parameter model in VSD variables.

The explicit expression of the constant matrices \mathbf{L}_{vsd} , \mathbf{M}_{vsd} can be found from (19) and, with a symbolic math tool, they can be easily checked to be:

$$\mathbf{L}_{vsd} = \begin{pmatrix} \mathbf{I}_2 \lambda_1 & \mathbf{0}_{2 \times 2} & \mathbf{0}_{2 \times 2} & \mathbf{0}_{2 \times 2} & \mathbf{0}_{2 \times 1} \\ \mathbf{0}_{2 \times 2} & \mathbf{I}_2 \lambda_3 & \mathbf{0}_{2 \times 2} & \mathbf{0}_{2 \times 2} & \mathbf{0}_{2 \times 1} \\ \mathbf{0}_{2 \times 2} & \mathbf{0}_{2 \times 2} & \mathbf{I}_2 \lambda_5 & \mathbf{0}_{2 \times 2} & \mathbf{0}_{2 \times 1} \\ \mathbf{0}_{2 \times 2} & \mathbf{0}_{2 \times 2} & \mathbf{0}_{2 \times 2} & \mathbf{I}_2 \lambda_7 & \mathbf{0}_{2 \times 1} \\ \mathbf{0}_{1 \times 2} & \mathbf{0}_{1 \times 2} & \mathbf{0}_{1 \times 2} & \mathbf{0}_{1 \times 2} & \lambda_9 \end{pmatrix} \quad (21)$$

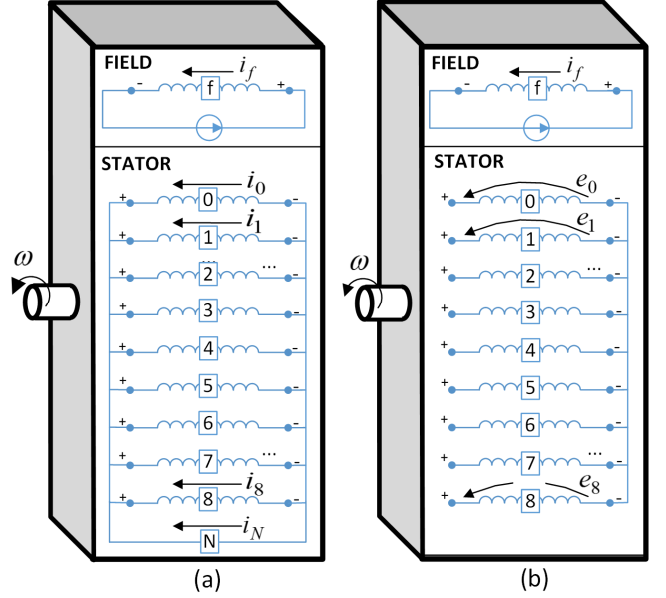


Fig. 2. Stator phases and rotor field circuit (a) in short circuit conditions; (b) at no-load conditions.

$$\mathbf{M}_{vsd} = \begin{pmatrix} \Gamma_{1,1} & \Gamma_{1,3} & \Gamma_{1,5} & \Gamma_{1,7} & \mathbf{0}_{2 \times 1} \\ \Gamma_{1,3} & \Gamma_{3,3} & \Gamma_{3,5} & \Gamma_{3,7} & \mathbf{0}_{2 \times 1} \\ \Gamma_{1,5} & \Gamma_{3,5} & \Gamma_{5,5} & \Gamma_{5,7} & \mathbf{0}_{2 \times 1} \\ \Gamma_{1,7} & \Gamma_{3,7} & \Gamma_{5,7} & \Gamma_{7,7} & \mathbf{0}_{2 \times 1} \\ \mathbf{0}_{1 \times 2} & \mathbf{0}_{1 \times 2} & \mathbf{0}_{1 \times 2} & \mathbf{0}_{1 \times 2} & 0 \end{pmatrix} \quad (22)$$

where: \mathbf{I}_2 is the 2×2 identity matrix, parameters $\lambda_1, \lambda_3, \lambda_5, \lambda_7, \lambda_9$ in (21) can be expressed in terms of the phase leakage inductances l_0, l_1, l_2, l_3, l_4 as

$$\lambda_h = l_0 + 2 \sum_{k=1,2,3,4} l_k \cos(hk \frac{\pi}{9}), \quad h \in \{1, 3, 5, 7, 9\} \quad (23)$$

and the 2×2 sub-matrices in (22) take the following form:

$$\Gamma_{i,j} = \frac{9\pi R L \mu_0}{4} \left[\begin{pmatrix} F_i W_j (P_{i-j} + P_{i+j}) & 0 \\ 0 & F_i W_j (P_{i-j} - P_{i+j}) \end{pmatrix} + \delta_{i,j} \begin{pmatrix} F_i W_i P_0 & 0 \\ 0 & F_i W_i P_0 \end{pmatrix} \right], \quad i, j \in \{1, 3, 5, 7, 9\} \quad (24)$$

where $i, j \in \{1, 3, 5, 7\}$ and F_s, W_s, P_k are the Fourier coefficients appearing in (6) and computed as per [22], with $\delta_{i,j}$ standing for Kronecker symbol:

$$\delta_{i,j} = \begin{cases} 1 & \text{if } i = j \\ 0 & \text{if } i \neq j \end{cases} \quad (25)$$

III. MODEL PARTICULARIZATION IN STEADY-STATE SHORT-CIRCUIT CONDITIONS

The machine model derived in the previous section through VSD can be particularized to the case of machine operation in steady-state (sustained) short-circuit conditions, as depicted in Fig. 2a in case of a wound-field synchronous machine. In Fig. 2a, i_0, i_1, \dots, i_8 denote the nine phase currents when the machine operates at an electrical speed ω in steady-state short-circuit conditions with a field current i_f . With the same field current i_f and at the same speed ω the phase back-emf's e_1, e_2, \dots, e_8 are induced in stator phases at no load (Fig. 2b).

At steady-state, the short circuit currents and back-emf's can be written as follows:

$$i_j(t) = [\mathbf{i}_{ph}(t)]_j = \sum_{k=1,3,5,7,9} I_k \cos[k(\omega t - \frac{\pi}{9} j) + \phi_k] \quad (26)$$

$$e_j(t) = [\mathbf{e}_{ph}(t)]_j = - \sum_{k=1,3,5,7,9} E_k \sin[k(\omega t - \frac{\pi}{9} j)] \quad (27)$$

where $j \in \{0,1,\dots,8\}$ is the phase index and $k \in \{1,3,5,7,9\}$ is the harmonic order; the terminal voltage is imposed to be zero on each stator phase due to the neutral connection indicated with the letter "N" in Fig. 2a. In (26)-(27), harmonic components up to the ninth order have been considered.

By transforming (26), (27) through (14) we obtain:

$$\mathbf{i}_{vsd} = \frac{3}{\sqrt{2}} \begin{pmatrix} I_1 \cos \phi_1 \\ I_1 \sin \phi_1 \\ I_3 \cos \phi_3 \\ I_3 \sin \phi_3 \\ I_5 \cos \phi_5 \\ I_5 \sin \phi_5 \\ I_7 \cos \phi_7 \\ I_7 \sin \phi_7 \\ \sqrt{2} I_9 \cos(9\omega t + \phi_9) \end{pmatrix}, \quad \mathbf{e}_{vsd} = \frac{3}{\sqrt{2}} \begin{pmatrix} 0 \\ E_1 \\ 0 \\ E_3 \\ 0 \\ E_5 \\ 0 \\ E_7 \\ \sqrt{2} E_9 \cos(9\omega t) \end{pmatrix} \quad (28)$$

In steady-state short-circuit conditions, the transformed machine equation (20) yields ($\mathbf{v}_{vsd} = \mathbf{0}$):

$$-\mathbf{e}_{vsd} = r_s \mathbf{i}_{vsd} + \omega \mathbf{J}(\mathbf{L}_{vsd} + \mathbf{M}_{vsd}) \mathbf{i}_{vsd} + (\mathbf{L}_{vsd} + \mathbf{M}_{vsd}) \frac{d}{dt} \mathbf{i}_{vsd} \quad (29)$$

It can be noted that all the elements of the transformed current and back-emf vectors (28) are constant except for the last one (accounting for the ninth harmonic), which is time dependent. In particular we can write:

$$\frac{d}{dt} \mathbf{i}_{vsd} = \begin{pmatrix} 0 \\ \vdots \\ 0 \\ -27\omega I_9 \sin(9\omega t + \phi_9) \end{pmatrix} \quad (30)$$

Furthermore, from (21)-(22) and considering (30), we can write:

$$(\mathbf{L}_{vsd} + \mathbf{M}_{vsd}) \frac{d}{dt} \mathbf{i}_{vsd} = \begin{pmatrix} 0 \\ \vdots \\ 0 \\ -27\omega \lambda_9 I_9 \sin(9\omega t + \phi_9) \end{pmatrix} \quad (31)$$

$$\omega \mathbf{J}(\mathbf{L}_{vsd} + \mathbf{M}_{vsd}) \mathbf{i}_{vsd} = \begin{pmatrix} * \\ \vdots \\ * \\ 0 \end{pmatrix} \quad (32)$$

where the symbol "*" denotes a number which is, in general, different from zero.

IV. LEAKAGE INDUCTANCE IDENTIFICATION FROM OPEN-CIRCUIT AND SHORT-CIRCUIT TESTS

In order to identify leakage inductances, a short circuit test is performed on the machine arranged according to the scheme shown in Fig. 2a at electrical speed ω and with a field current i_f ; a no-load test (Fig. 2b) is also performed on the machine at the same electrical speed ω and with the same field current i_f . In the short circuit test, one phase current (e.g. i_0) is recorded and its Fourier series coefficients I_1, I_3, I_5, I_7, I_9 are extracted from the measurement.

Moreover, the no-load voltage of one phase (e.g. e_0) is recorded in the no-load test and its Fourier series coefficients E_1, E_3, E_5, E_7, E_9 are extracted from the measurement. In this way, the transformed current and back-emf vectors (28) are known except for the phase angles $\phi_1, \phi_3, \phi_5, \phi_7, \phi_9$.

The idea is therefore to use the measured Fourier coefficients E_1, E_3, E_5, E_7, E_9 and I_1, I_3, I_5, I_7, I_9 to identify the leakage inductance matrix \mathbf{L}_{vsd} (21) in (29) and, from the knowledge of parameters $\lambda_1, \lambda_3, \lambda_5, \lambda_7, \lambda_9$, to finally

determine the physical stator leakage inductances l_0, l_1, l_2, l_3, l_4 through (23).

For this purpose, based on (30)-(32) we can observe that (29) is equivalent to the system of the following two equations ("~" denotes reduced-order matrices and vectors):

$$\begin{cases} -\tilde{\mathbf{e}}_{vsd} = r_s \tilde{\mathbf{i}}_{vsd} + \omega \tilde{\mathbf{J}}(\tilde{\mathbf{L}}_{vsd} + \tilde{\mathbf{M}}_{vsd}) \tilde{\mathbf{i}}_{vsd} \\ -E_9 \cos(9\omega t) = r_s I_9 \cos(9\omega t + \phi_9) - 9\omega \lambda_9 I_9 \sin(9\omega t + \phi_9) \end{cases} \quad (33)$$

where

$$\tilde{\mathbf{i}}_{vsd} = \frac{3}{\sqrt{2}} \begin{pmatrix} I_1 \cos \phi_1 \\ I_1 \sin \phi_1 \\ I_3 \cos \phi_3 \\ I_3 \sin \phi_3 \\ I_5 \cos \phi_5 \\ I_5 \sin \phi_5 \\ I_7 \cos \phi_7 \\ I_7 \sin \phi_7 \end{pmatrix}, \quad \tilde{\mathbf{e}}_{vsd} = \frac{3}{\sqrt{2}} \begin{pmatrix} 0 \\ E_1 \\ 0 \\ E_3 \\ 0 \\ E_5 \\ 0 \\ E_7 \end{pmatrix} \quad (34)$$

$$\tilde{\mathbf{L}}_{vsd} = \begin{pmatrix} \mathbf{I}_{2 \times 2} \lambda_1 & \mathbf{0}_{2 \times 2} & \mathbf{0}_{2 \times 2} & \mathbf{0}_{2 \times 2} \\ \mathbf{0}_{2 \times 2} & \mathbf{I}_{2 \times 2} \lambda_3 & \mathbf{0}_{2 \times 2} & \mathbf{0}_{2 \times 2} \\ \mathbf{0}_{2 \times 2} & \mathbf{0}_{2 \times 2} & \mathbf{I}_{2 \times 2} \lambda_5 & \mathbf{0}_{2 \times 2} \\ \mathbf{0}_{2 \times 2} & \mathbf{0}_{2 \times 2} & \mathbf{0}_{2 \times 2} & \mathbf{I}_{2 \times 2} \lambda_7 \end{pmatrix}, \quad \tilde{\mathbf{M}}_{vsd} = \begin{pmatrix} \Gamma_{1,1} & \Gamma_{1,3} & \Gamma_{1,5} & \Gamma_{1,7} \\ \Gamma_{1,3} & \Gamma_{3,3} & \Gamma_{3,5} & \Gamma_{3,7} \\ \Gamma_{1,5} & \Gamma_{3,5} & \Gamma_{5,5} & \Gamma_{5,7} \\ \Gamma_{1,7} & \Gamma_{3,7} & \Gamma_{5,7} & \Gamma_{7,7} \end{pmatrix} \quad (35)$$

The first equation in (33) will be used to determine the unknown coefficients $\lambda_1, \lambda_3, \lambda_5, \lambda_7$ (IV.A), the second to determine the coefficient λ_9 (IV.B) and, finally, the leakage inductances l_0, l_1, l_2, l_3, l_4 will be obtained from $\lambda_1, \lambda_3, \lambda_5, \lambda_7, \lambda_9$ (IV.C).

A. Determination of $\lambda_1, \lambda_3, \lambda_5, \lambda_7$

The first (matrix) equation in (33) can be put in the following form:

$$\mathbf{F}(\lambda_1, \lambda_3, \lambda_5, \lambda_7) \tilde{\mathbf{e}}_{vsd} = \tilde{\mathbf{i}}_{vsd} \quad (36)$$

where

$$\mathbf{F}(\lambda_1, \lambda_3, \lambda_5, \lambda_7) = -\{r_s \mathbf{I}_8 + \omega \tilde{\mathbf{J}}(\tilde{\mathbf{L}}_{vsd} + \tilde{\mathbf{M}}_{vsd})\}^{-1} \quad (37)$$

pointing out that the matrix \mathbf{F} depends on the four unknown parameters $\lambda_1, \lambda_3, \lambda_5, \lambda_7$, included in $\tilde{\mathbf{L}}_{vsd}$.

At this point, we introduce the auxiliary constant matrices:

$$\mathbf{U}_1 = \begin{pmatrix} \mathbf{I}_2 \\ \mathbf{0}_{2 \times 2} \\ \mathbf{0}_{2 \times 2} \\ \mathbf{0}_{2 \times 2} \end{pmatrix}, \quad \mathbf{U}_3 = \begin{pmatrix} \mathbf{0}_{2 \times 2} \\ \mathbf{I}_2 \\ \mathbf{0}_{2 \times 2} \\ \mathbf{0}_{2 \times 2} \end{pmatrix}, \quad \mathbf{U}_5 = \begin{pmatrix} \mathbf{0}_{2 \times 2} \\ \mathbf{0}_{2 \times 2} \\ \mathbf{I}_2 \\ \mathbf{0}_{2 \times 2} \end{pmatrix}, \quad \mathbf{U}_7 = \begin{pmatrix} \mathbf{0}_{2 \times 2} \\ \mathbf{0}_{2 \times 2} \\ \mathbf{0}_{2 \times 2} \\ \mathbf{I}_2 \end{pmatrix} \quad (38)$$

By left-multiplying (37) by the transposed matrices (38) we obtain:

$$\mathbf{U}_k^t \mathbf{F}(\lambda_1, \lambda_3, \lambda_5, \lambda_7) \tilde{\mathbf{e}}_{vsd} = \mathbf{U}_k^t \tilde{\mathbf{i}}_{vsd} = \begin{pmatrix} I_k \cos \phi_k \\ I_k \sin \phi_k \end{pmatrix} \quad (39)$$

for any $k \in \{1,3,5,7\}$. Hence:

$$\begin{aligned} [\mathbf{U}_k^t \mathbf{F}(\lambda_1, \lambda_3, \lambda_5, \lambda_7) \tilde{\mathbf{e}}_{vsd}]^t [\mathbf{U}_k^t \mathbf{F}(\lambda_1, \lambda_3, \lambda_5, \lambda_7) \tilde{\mathbf{e}}_{vsd}] &= \\ = \tilde{\mathbf{e}}_{vsd}^t \mathbf{F}(\lambda_1, \lambda_3, \lambda_5, \lambda_7)^t \mathbf{U}_k \mathbf{U}_k^t \mathbf{F}(\lambda_1, \lambda_3, \lambda_5, \lambda_7) \tilde{\mathbf{e}}_{vsd} &= \\ = \tilde{\mathbf{e}}_{vsd}^t \mathbf{F}(\lambda_1, \lambda_3, \lambda_5, \lambda_7)^t \mathbf{E}_k \mathbf{F}(\lambda_1, \lambda_3, \lambda_5, \lambda_7) \tilde{\mathbf{e}}_{vsd} &= \\ = \begin{pmatrix} I_k \cos \phi_k \\ I_k \sin \phi_k \end{pmatrix}^t \begin{pmatrix} I_k \cos \phi_k \\ I_k \sin \phi_k \end{pmatrix} = I_k^2 & \end{aligned} \quad (40)$$

where

$$\mathbf{E}_k = \begin{pmatrix} \mathbf{I}_{2 \times 2} \delta_{1,k} & \mathbf{0}_{2 \times 2} & \mathbf{0}_{2 \times 2} & \mathbf{0}_{2 \times 2} \\ \mathbf{0}_{2 \times 2} & \mathbf{I}_{2 \times 2} \delta_{3,k} & \mathbf{0}_{2 \times 2} & \mathbf{0}_{2 \times 2} \\ \mathbf{0}_{2 \times 2} & \mathbf{0}_{2 \times 2} & \mathbf{I}_{2 \times 2} \delta_{5,k} & \mathbf{0}_{2 \times 2} \\ \mathbf{0}_{2 \times 2} & \mathbf{0}_{2 \times 2} & \mathbf{0}_{2 \times 2} & \mathbf{I}_{2 \times 2} \delta_{7,k} \end{pmatrix} \quad (41)$$

being $\delta_{i,j}$ Kronecker symbol defined by (25).

In conclusion, (40) yields the following set of equations:

$$\begin{cases} \tilde{\mathbf{e}}_{vsd}^t \mathbf{F}(\lambda_1, \lambda_3, \lambda_5, \lambda_7)^t \mathbf{E}_1 \mathbf{F}(\lambda_1, \lambda_3, \lambda_5, \lambda_7) \tilde{\mathbf{e}}_{vsd} = I_1^2 \\ \tilde{\mathbf{e}}_{vsd}^t \mathbf{F}(\lambda_1, \lambda_3, \lambda_5, \lambda_7)^t \mathbf{E}_3 \mathbf{F}(\lambda_1, \lambda_3, \lambda_5, \lambda_7) \tilde{\mathbf{e}}_{vsd} = I_3^2 \\ \tilde{\mathbf{e}}_{vsd}^t \mathbf{F}(\lambda_1, \lambda_3, \lambda_5, \lambda_7)^t \mathbf{E}_5 \mathbf{F}(\lambda_1, \lambda_3, \lambda_5, \lambda_7) \tilde{\mathbf{e}}_{vsd} = I_5^2 \\ \tilde{\mathbf{e}}_{vsd}^t \mathbf{F}(\lambda_1, \lambda_3, \lambda_5, \lambda_7)^t \mathbf{E}_7 \mathbf{F}(\lambda_1, \lambda_3, \lambda_5, \lambda_7) \tilde{\mathbf{e}}_{vsd} = I_7^2 \end{cases} \quad (42)$$

which is a system of four nonlinear equations in the four unknowns $\lambda_1, \lambda_3, \lambda_5, \lambda_7$. The system can be solved numerically, e.g. with conjugate gradient method [26].

B. Determination of λ_9

The parameter λ_9 can be determined from the second equation in the system (33). We can define the quantity:

$$Z_9 = \sqrt{r_s^2 + (9\omega\lambda_9)^2} \quad (43)$$

and the angle ψ_9 such that

$$\cos\psi_9 = \frac{r_s}{Z_9}, \quad \sin\psi_9 = \frac{9\omega\lambda_9}{Z_9}. \quad (44)$$

By dividing both members of the second equation in system (33) by Z_9 we obtain:

$$\begin{aligned} -\frac{E_9}{Z_9} \cos(9\alpha) &= \frac{r_s}{Z_9} I_9 \cos(9\alpha + \phi_9) - \frac{9\omega\lambda_9}{Z_9} I_9 \sin(9\alpha + \phi_9) = \\ &= I_9 \cos(\psi_9) \cos(9\alpha + \phi_9) - I_9 \sin(\psi_9) \sin(9\alpha + \phi_9) = \\ &= I_9 \cos(9\alpha + \phi_9 + \psi_9) \end{aligned} \quad (45)$$

In order for the first and last member of (45) to be equal, the following identities must hold:

$$\phi_9 + \psi_9 = \pi, \quad (46)$$

$$Z_9 = \frac{E_9}{I_9} \quad (47)$$

Considering the expression (43) for Z_9 , (47) implies:

$$\lambda_9 = \frac{\sqrt{(E_9/I_9)^2 - r_s^2}}{9\omega} \quad (48)$$

which gives the value of the parameter λ_9 .

C. Determination of l_0, l_1, l_2, l_3, l_4

Once parameters $\lambda_1, \lambda_3, \lambda_5, \lambda_7, \lambda_9$ are known, the physical leakage inductances l_0, l_1, l_2, l_3, l_4 can be determined based on the linear relationship (23), which can be written in matrix form as follows:

$$(\lambda_1 \ \lambda_3 \ \lambda_5 \ \lambda_7 \ \lambda_9)^t = \mathbf{A} (l_0 \ l_1 \ l_2 \ l_3 \ l_4)^t \Rightarrow \quad (49)$$

$$\Rightarrow (l_0 \ l_1 \ l_2 \ l_3 \ l_4)^t = \mathbf{A}^{-1} (\lambda_1 \ \lambda_3 \ \lambda_5 \ \lambda_7 \ \lambda_9)^t \quad (50)$$

where the matrix \mathbf{A} is given by (51) and is certainly invertible as its determinant is equal to $|\mathbf{A}|=243$.

$$\mathbf{A} = \begin{pmatrix} 1 & 2\cos(\alpha) & 2\cos(2\alpha) & 2\cos(3\alpha) & 2\cos(4\alpha) \\ 1 & 2\cos(3\alpha) & 2\cos(6\alpha) & 2\cos(9\alpha) & 2\cos(12\alpha) \\ 1 & 2\cos(5\alpha) & 2\cos(10\alpha) & 2\cos(15\alpha) & 2\cos(20\alpha) \\ 1 & 2\cos(7\alpha) & 2\cos(14\alpha) & 2\cos(21\alpha) & 2\cos(28\alpha) \\ 1 & 2\cos(9\alpha) & 2\cos(18\alpha) & 2\cos(27\alpha) & 2\cos(36\alpha) \end{pmatrix} \quad (51)$$

V. PRACTICAL APPLICATION EXAMPLE

In order to illustrate and assess the proposed procedure the nine-phase generator shown in Fig. 3 and Fig. 4 is used. Its ratings are reported in Table I and its main electromagnetic design data are provided in Table II.

TABLE I. MACHINE RATINGS

Rated power	21 kVA
Rated power factor	0.8
Rated speed	3000 rpm
Rated voltage	500 V
Number of poles	2

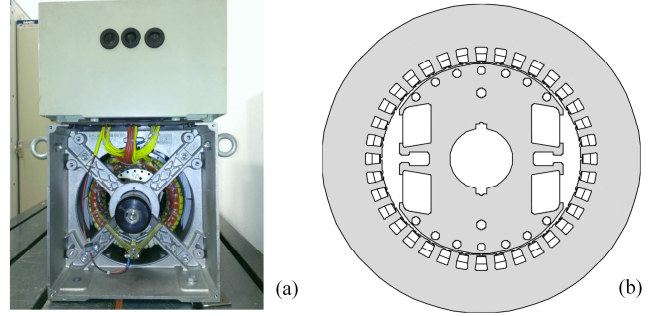


Fig. 3. Generator used for testing: (a) picture; (b) cross section.

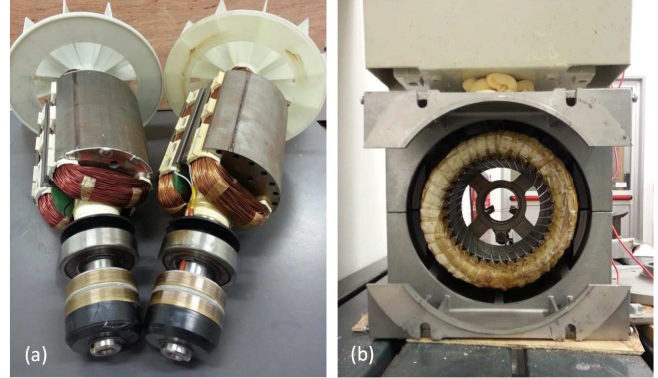


Fig. 4. Pictures of: (a) the two rotors used for testing (with and without damper cage); (b) stator with the rotor removed.

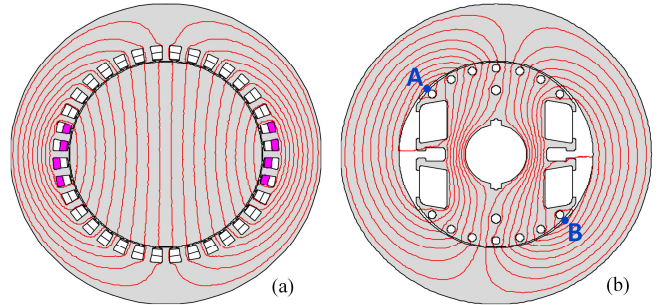


Fig. 5. Results of the FEA simulations needed for magnetizing inductance identification.

TABLE II. ELECTROMAGNETIC DESIGN DATA

Core length	150 mm
Stator bore inner radius, R_i	75 mm
Minimum air-gap width, g	0.8 mm
Number of stator slots	36
Number of turns per stator coil, N_c	21
Coil pitch, γ	(16/18) π
Number parallel paths per phase, b	1
Number of excitation winding turns	540
Number of slots/pole/phase, q	2
Mean air-gap radius, R	37.1 mm
Stator phase resistance at 20°C, r_s	1.86 Ω

The application of the proposed procedure to the machine selected for testing includes the steps described in the next subsections.

A. Computation of magnetizing inductance parameters

The first step consists of computing the magnetizing inductances $m_{ij}(\theta)$ in the Fourier series expansion form given by (6). The procedure described in [22] is adopted, which enables one to identify all the Fourier coefficients F_s, W_r, P_k based on some analytical formulas and through a couple of magneto-static FEA simulations. More precisely, coefficients W_r are computed as:

$$W_r = \frac{4 N_c}{\pi b} \frac{\sin(r\gamma/2) \sin(\alpha_s q r / 2)}{r \sin(\alpha_s r / 2)} \quad (52)$$

where

$$\alpha_s = \pi / (9q) \quad (53)$$

being: N_c the number of stator turns per coil, b the number of parallel paths per phase, γ the coil pitch in electrical radians, q the number of slots per pole per phase, α_s the slot pitch in electrical radians.

As regards coefficients F_s, P_k , they are derived, based on [22], from the post-processing of the two FEA simulations shown in Fig. 5. In particular:

- The model used in Fig. 5a features the same stator as that of the real machine, while the rotor is replaced by a round one so as to have a uniform air-gap g equal to the minimum air-gap of the real machine. The model is energized by imposing an arbitrary current in one stator phase and then the radial magnetic field along the mean air-gap circumference is obtained and post-processed as discussed in [22] to obtain coefficients F_s .
- The model shown in Fig. 5b includes a slotless stator core with a bore radius R_s and a rotor geometry which are the same as for the real machine. The model is energized with the two punctual ideal conductors marked as A and B in Fig. 5b; the resulting radial magnetic field is then computed and post-processed as discussed in [22] to determine coefficients P_k .

The non-dimensional coefficients F_s, W_r, P_k obtained for the first (significant) values of indices s, r, k are reported in Table III and Table IV.

TABLE III. VALUES OF FOURIER COEFFICIENTS F_s AND W_s

s or r	1	3	5	7	9
F_s	45.97	-13.62	5.73	-1.977	4.245×10^{-3}
W_r	52.463	-14.9	6.231	-2.14	0

TABLE IV. VALUES OF FOURIER COEFFICIENTS P_k

k	P_k	k	P_k	k	P_k	k	P_k	k	P_k
0	0.442	4	0.025	8	0.050	12	$3.3 \cdot 10^{-3}$	16	-0.012
2	0.446	6	0.019	10	-0.020	14	0.021	18	$1.1 \cdot 10^{-3}$

The knowledge of parameters F_s, W_r, P_k leads to fully identify the magnetizing self and mutual inductances given by (6) and to fully determine the magnetizing inductance $\tilde{\mathbf{M}}_{vsd}$ through its submatrices $\Gamma_{i,j}$ given by (24).

B. No-load and short circuit tests

The following step is to perform the no-load and the sustained short circuit tests on the built machine [18]. It is essential that both these tests are conducted at the same speed ω and with the same excitation current i_f (Fig. 2). Furthermore, during the short-circuit test, the phase terminals need not only to be shorted, but also connected to the star point through a negligible-impedance wire indicated with letter “N” in Fig. 2a. This is necessary to let the third and ninth current harmonics flow in machine phases.

In the no-load test, the open-circuit voltage waveform across a machine phase is recorded. For example, on the machine shown in Fig. 3 and Fig. 4 the no-load test is conducted at 1500 rpm ($\omega=157$ rad/s) with a DC field excitation current $i_f=1.58$ A and the waveform shown in Fig. 6 is recorded. By spectral analysis of the recorded waveform, the back-emf Fourier coefficients E_k ($k=1, 3, \dots, 9$) appearing in (27) and (28) are obtained. Their values are given in Table V.

In the short-circuit test, the current waveform is recorded and then analyzed to identify the magnitudes of coefficients

I_k ($k=1, 3, \dots, 9$) appearing in (26) and (28). Their values are given in Table V. The recorded waveform and its reconstruction are shown in Fig. 7.

TABLE V. FOURIER COEFFICIENTS E_k AND I_k FROM THE NO-LOAD AND SHORT-CIRCUIT TESTS

k	1	3	5	7	9
E_k (V)	124.4	-26.7	-1.9	-3.1	$5.1 \cdot 10^{-3}$
$ I_k $ (A)	2.06	1.23	0.62	0.57	$2.3 \cdot 10^{-3}$

It is worth noting that the transformed back-emf vector \mathbf{e}_{vsd} in (28) is fully identified from the no-load test through the computation of coefficients E_k , while the short circuit current vector \mathbf{i}_{vsd} in (28) is not completely known because, from the short-circuit test, the magnitudes of coefficients I_k can be easily determined while the phase angles ϕ_k are undetermined. The reason for this is illustrated in Fig. 8 which highlights that the back-emf fundamental is certainly aligned with the q axis [consistently with (27), (28)], while the fundamental of the short circuit current is shifted by ϕ_1 with respect to the d axis [consistently with

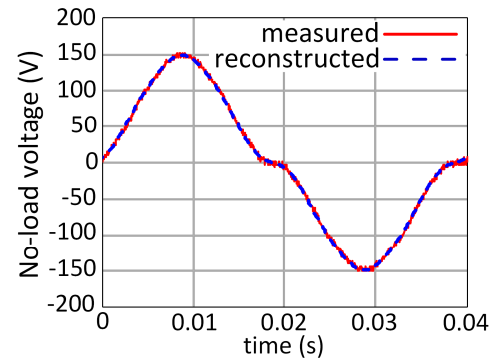


Fig. 6. Open-circuit voltage waveform recorded on the test machine at 1500 rpm with a field excitation current of 1.58 A. The reconstructed waveform uses Fourier coefficients given in Table V.

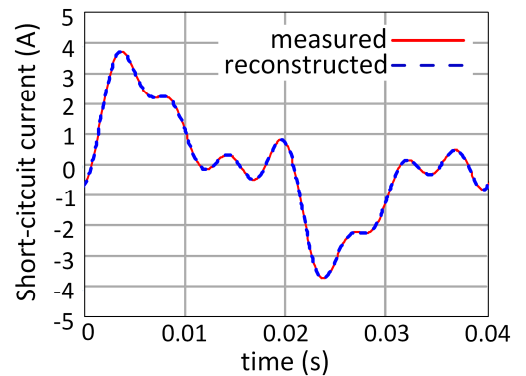


Fig. 7. Short-circuit current waveform recorded in the sustained short circuit test at 1500 rpm with a field excitation current of 1.58 A. The reconstructed waveform uses Fourier coefficients given in Table V.

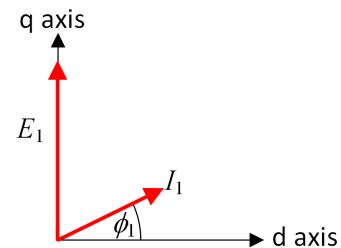


Fig. 8. Phasor diagram for the back-emf and short circuit current fundamentals in the machine dq reference frame.

(26), (28)] and by $\pi - \phi_l$ with respect to the fundamental of the back-emf; however, in the short circuit test, neither the rotor position (i.e. the d axis position) nor the back-emf signal are available, hence ϕ_l remains undetermined together with the other phase angles $\phi_3, \phi_5, \phi_7, \phi_9$.

C. Identification of parameters $\lambda_1, \lambda_3, \lambda_5, \lambda_7, \lambda_9$

1) Parameters $\lambda_1, \lambda_3, \lambda_5, \lambda_7$

Based on the no-load and short circuit tests, the vector $\tilde{\mathbf{e}}_{vsd}$ in (34) is known as well as the values of $|I_1|, |I_3|, |I_5|, |I_7|$. On the other side, the matrix $\tilde{\mathbf{M}}_{vsd}$ is also fully identified as described in V.A and therefore, supposing that also the stator phase resistance r_s is known (Table II), the matrix \mathbf{F} defined by (37) is a function of the only unknown parameters $\lambda_1, \lambda_3, \lambda_5, \lambda_7$. As a result, the set of equations in (42) is a nonlinear system in the only unknowns $\lambda_1, \lambda_3, \lambda_5, \lambda_7$. This system can be solved with numerical methods [26]. In the case of the test machine considered in this paper, the numerical solution (42), performed with the conjugate gradient method, gives the results shown in Table VI. The same table also shows the initial guess values of the unknowns used for the numerical solution of (42).

TABLE VI. PARAMETERS $\lambda_1, \lambda_3, \lambda_5, \lambda_7$

	λ_1	λ_3	λ_5	λ_7	λ_9
Initial guess (mH)	10	10	10	10	—
Identified values (mH)	7.78	1.92	0.88	1.16	0.85

2) Parameter λ_9

The identification of the parameter λ_9 does not require any numerical procedure as it can be performed by means of (48) using the measured voltage and current components E_9 and $|I_9|$ (Table V) and the phase resistance r_s (Table II). This gives the value of λ_9 given in Table VI.

3) Parameter identification check

Once all the five values $\lambda_1, \lambda_3, \lambda_5, \lambda_7, \lambda_9$ are determined, all the parameters of the machine model in VSD coordinates are known. It is then possible to check the correctness of the parameter identification by computing the short circuit current from (29), which gives the block-scheme diagram shown in Fig. 9. As a solution, the phase short circuit current vector \mathbf{i}_{ph} is obtained at steady-state. One phase current is plotted in Fig. 10 and shown to almost perfectly match the measured current waveform. The same figure also shows the current waveform obtained by setting the parameters $\lambda_1, \lambda_3, \lambda_5, \lambda_7, \lambda_9$ equal to their initial-guess values (Table VI). It can be seen that the latter waveform strongly differ from the measured one. This confirms the importance of the leakage parameters $\lambda_1, \lambda_3, \lambda_5, \lambda_7, \lambda_9$ in determining the short circuit current waveform and proves that the identified values (Table VI) have been correctly determined.

D. Computation of physical phase leakage inductances

As a final step, the physical self and mutual leakage inductances l_0, l_1, l_2, l_3, l_4 are determined by solution of the linear system (50). The numerical values obtained are given in Table VII, which shows the result of the stator leakage inductance identification procedure when the two kinds of rotors shown in Fig. 4a (one with and the other without the damper cage) are used in the no-load and short circuit tests (V.A, V.B).

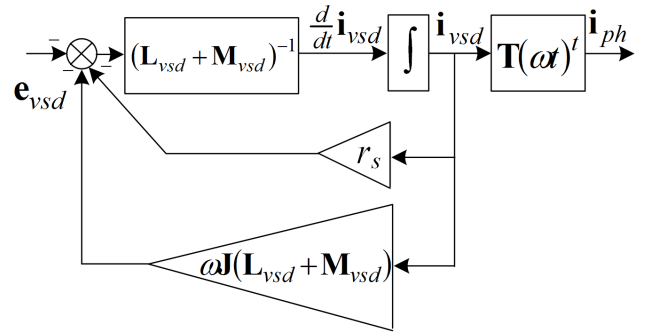


Fig. 9. Block diagram for the computation of the short circuit current in phase variables \mathbf{i}_{ph} .

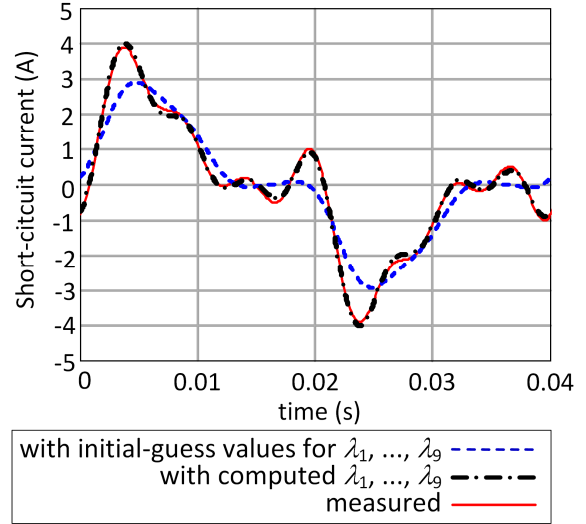


Fig. 10. Short circuit current waveform: measured; before leakage inductance identification; after leakage inductance identification.

TABLE VII. STATOR PHYSICAL LEAKAGE INDUCTANCES l_0, l_1, l_2, l_3, l_4 (mH) IDENTIFIED WITH TWO DIFFERENT KINDS OF ROTOR

Rotor type	l_0	l_1	l_2	l_3	l_4
Without dampers	2.70	1.52	1.06	0.57	0.08
With dampers	2.75	1.47	1.09	0.60	0.08

Table VII demonstrates that the presence of rotor circuits does not significantly impact on the results of the stator leakage inductance identification procedure. This is also confirmed by the fact that the no-load and short circuit current waveforms are practically the same as shown in Fig. 6 and Fig. 7, respectively, for both kinds of rotors.

The independency of stator leakage identification results on the rotor circuits is important as it justifies the usage of a machine model (Sections II, III) where no rotor-related parameters are used and where only the no-load back-emf appears.

The reason why rotor circuits do not impact on the proposed identification procedure is theoretically simple to justify. In fact, the no-load voltage is the same regardless of whether the rotor is equipped or not with a damper cage. Furthermore, the significant harmonics which appear in the short circuit current (with orders from 3 to 9) are known to not produce any resultant air-gap flux since their magnetomotive force fields mutually cancel out [2], [11], [13]. Hence, neglecting the current harmonics with higher harmonic orders than the ninth, the damper cage during the short circuit test does not react, if present, and therefore the overall machine behaves as if the dampers were not present. This has been also experimentally validated in [27].

VI. EXPERIMENTAL VALIDATION AND COMPARISON WITH FEA RESULTS

A. Experimental validations against measurements on the machine with the rotor removed

The stator leakage inductance identification method proposed in this paper is not easy to validate experimentally due to the lack of well-established methods or standards for the measurement of stator leakage inductances. The most reliable alternative way to perform such measurement to be used for comparison has been derived from the test with the rotor removed proposed in [18] for stator leakage inductance determination in three-phase machines. The same procedure has been already adopted in [19] for determining the stator end-coil leakage inductance of a three-phase turbo-alternator and in [20]-[21] for the experimental determination of end-coil [20] and end-coil plus slot [21] leakage inductances of machines with various phase counts.

This experimental procedure is applied to the test generator shown in Fig. 4 and Fig. 5. This leads to measure the physical inductance values l_0, l_1, l_2, l_3, l_4 given in the histogram in Fig. 11. In the diagram, the direct measurements obtained from the test with the rotor removed are compared to the values obtained with the methodology proposed in this paper (Sections IV, V). It can be seen that a satisfactory matching is achieved.

B. Comparison with FEA results

It is reasonable to investigate if 2D FEA, which is used to determine magnetizing inductances, could be effectively used for a full calculation of leakage inductances as well. For this purpose, inductances are calculated for the machine under test through 2D FEA by segregating the leakage terms l_0, l_1, l_2, l_3, l_4 from the magnetizing ones $m_{i,j}(\theta)$ according to the definitions provided in Section II.A.

1) Leakage inductance computation by FEA

The procedure followed is illustrated in Fig. 12 where the mutual inductance between phases “0” and “6” is taken as an example: the phase “0” is energized with a given current I , while the other phases and the field circuit are at no load; then the total flux $A_6(\theta)$ linked by phase “6” as a function of the rotor positions θ is computed by FEA. This gives the total mutual inductance between phases “0” and “6”, namely the quantity:

$$l_6 + m_{0,6}(\theta) = A_6 / I. \quad (54)$$

In order to segregate the leakage inductance terms l_6 , the magnetizing component $m_{0,6}(\theta)$ needs to be determined as

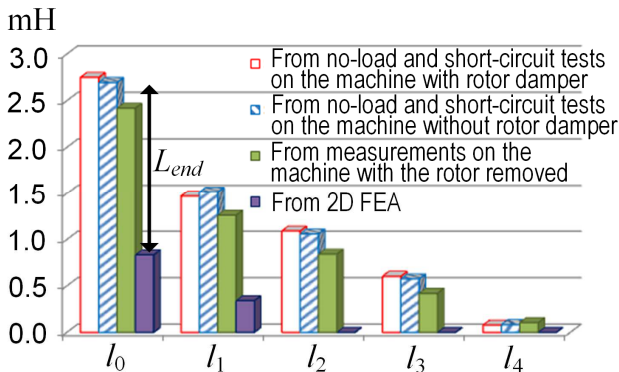


Fig. 11. Physical leakage inductance values obtained from the proposed identification method (on the machine with and without the rotor damper cage), from measurements on the machine with the rotor removed and from 2D FEA.

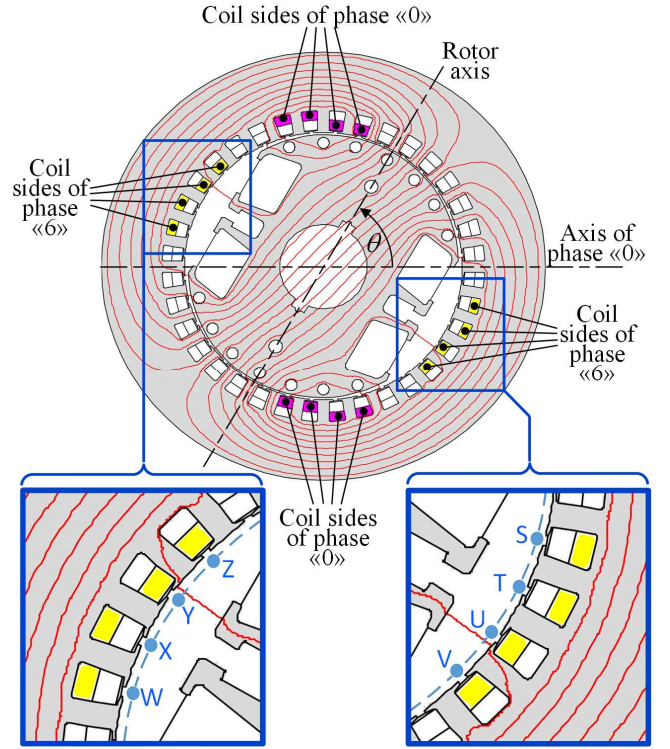


Fig. 11. Schematic illustrating the computation of total and magnetizing mutual inductances between phases “0” and “6” by 2D FEA when the rotor is placed at θ electrical radians with respect to the phase “0” axis.

well. This is done using the vector potential in the points S, T, U, V, W, X, Y, Z placed in the mean air-gap circumference of radius R in front of the slots including coils of phase “6”, as shown in Fig. 12. More precisely, $m_{0,6}(\theta)$ is computed as:

$$m_{0,6}(\theta) = L[A_S(\theta) + A_T(\theta) + A_U(\theta) + A_V(\theta) - A_W(\theta) - A_X(\theta) - A_Y(\theta) - A_Z(\theta)], \quad (55)$$

where $A_S(\theta)$ is the vector potential, computed by FEA, at point S (Fig. 12) when the rotor is at position θ and the same holds for the vector potentials in the other mentioned seven points.

The results of the inductance computations by 2D FEA are shown in Fig. 13 in the form of self-inductance of phase “0” and mutual inductances between phase “0” and phases “1”, “2”, “3” and “4”. The mutual inductance between phase “0” and phases “5”, “6”, “7” and “8” are omitted as they can be obtained from the displayed diagrams using the relationship:

$$l_j + m_{0,j}(\theta) = -\left[l_{9-j} + m_{0,9-j}\left(\theta - \frac{\pi}{9}j\right)\right]. \quad (56)$$

which can be easily proved based on symmetry considerations and also based on the theory in Section II.

From Fig. 13 it can be seen that the only two leakage inductances which (according to 2D FEA) take non-negligible values compared to magnetizing terms are l_0 and l_1 . This is due to the fact that the computed leakage inductances are essentially due to slot leakage flux (end-coil leakage phenomena not being captured by 2D FEA); hence, it is intuitively predictable that the only significant leakage inductances are the self-leakage inductance of each phase (l_0) and the mutual leakage inductance between adjacent phases (l_1), which have coil sides placed in the same slots [21].

The leakage inductances l_0, l_1, l_2, l_4 computed by 2D FEA with the procedure illustrated above are included in the

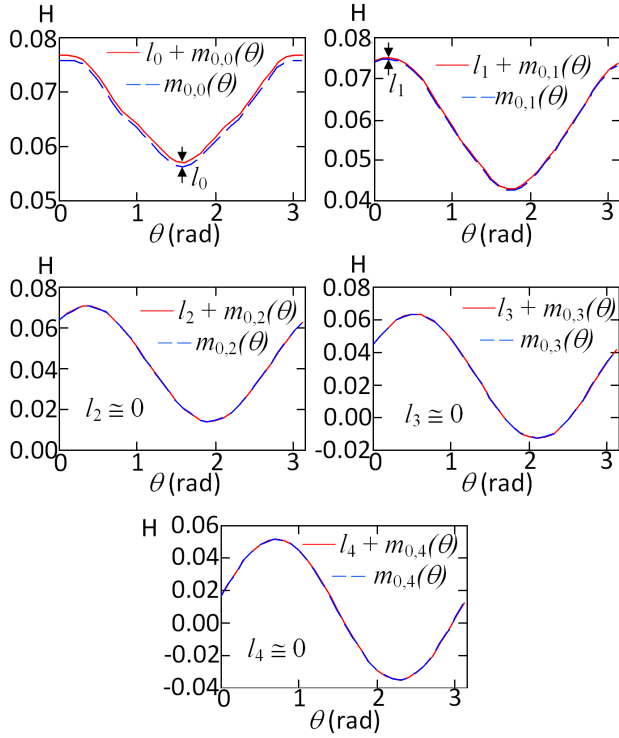


Fig. 13. Inductance values as functions of the rotor position computed by 2D FEA.

histogram shown in Fig. 11 for comparison with the same values obtained in other ways (i.e. from measurements on the machine with the rotor removed and from the post-processing of no-load and short-circuit tests). It can be seen that leakage inductance estimation by 2D FEA exhibits a very large error with respect to the other prediction methods. Hence, 2D FEA appears inadequate for the purpose of an accurate estimation of leakage inductances.

2) Interpretation of results and importance of end-coil effects

The discrepancies found in the estimation of the total leakage inductances by 2D FEA (Fig. 11) are due to the fact that 2D FEA can well account for slot leakage effects, but is incapable of capturing end-coil leakage fluxes. As discussed and experimentally proven in previous works [21], the end-coil leakage inductance can be comparable to (or even larger than) the slot leakage one. This is particularly likely to occur in those machine configurations (e.g. some two-pole designs) where the length of end coils is comparable to (or larger than) the length of the straight coil portions embedded in the slots.

The fact that the error in the leakage inductance evaluation by 2D FEA is due to end coil effects is proven by a dedicated experiment on the nine-phase machine used for validation. The experiment is performed on the machine after rotor removal and consists of placing a pre-formed search coil (composed on $N_s=2$ series-connected turns fixed on a plastic support) in the end-coil region as shown in Fig. 14. The angular span of the search coil in the circumferential direction is equal to the span of an end coil. The search coil terminals are connected to a voltage probe (Fig. 14) to measure the induced no-load electromotive force (emf) E_t . At this point, the phase “0” of the machine is energized with a current $I_t=8$ A rms at a frequency $f_t=50$ Hz (with the other phases at no load) and the search coil is moved circumferentially into the position where it links the maximum leakage flux, that is in the position where the emf

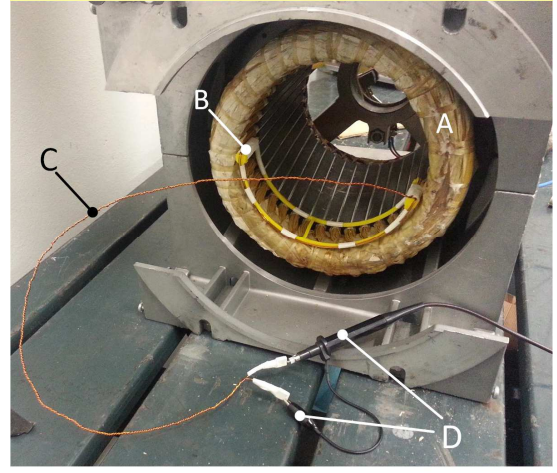


Fig. 12. Experimental set-up for the assessment of end-coil contribution to phase leakage inductances. A–End coils. B–Search coil. C–Search coil terminals (twisted to avoid flux linkages outside the search coil). D–Voltage probe connected to the oscilloscope.

in it is maximum. In this situation, the measured emf is $E_t=0.108$ V rms the flux linkage Λ_t of the search coil is evaluated as:

$$\Lambda_t = \frac{E_t}{2\pi f_t} = 3.44 \times 10^{-4} \text{ wb rms.} \quad (57)$$

From this measurement, the flux linkage Λ_{ec} due to the end coils of phase “0” on both machine sides is approximately estimated as:

$$\Lambda_{ec} = \Lambda_t \frac{2N_c q}{N_t} = 0.0144 \text{ wb rms.} \quad (58)$$

where: q and N_c are respectively the number of slots per pole per phase and the number of turns per coil for the machine; N_t is the number of turns in the search coil; the coefficient 2 at the numerator accounts for end coils being present on both machine sides.

Finally, the approximate estimation L_{end} of phase “0” self-inductance due to end coil leakage flux is derived dividing Λ_{ec} in (58) by the phase rms current I_t :

$$L_{end} = \frac{\Lambda_{ec}}{I_t} = 1.81 \times 10^{-3} \text{ H.} \quad (59)$$

The L_{end} value obtained in this way is reported in Fig. 11 (arrow) showing that the magnitude of L_{end} well matches the “gap” between the phase self leakage inductance estimated by FEA and the phase self leakage inductance estimated by the other methods. This confirms that 2D FEA does not suffice for a complete and accurate estimation of leakage inductance as it cannot capture end coil leakage effects, which can be seen to be definitely non-negligible in some machine designs, such as in the two-pole machine prototype used for validations in this paper.

3) Note on end coil leakage estimation by FEA

Finally, a note is included regarding the possibility to estimate the end-coil leakage inductance portion (not captured by 2D FEA) resorting to alternative techniques. Some hybrid numerical-analytical procedures have been proposed in the literature for this purpose, based on Neumann integrals and on the method of mirror images [19]-[20]. These techniques are well suited for turbo-alternators equipped with Roebel bars [19] and for winding designs based on preformed coils [20] since, in these cases, the end coil geometry is relatively easy to model and discretize into multiple straight elements for which an

analytical solution of Neumann integrals can be found [19]-[20]. Other kinds of stator designs (such as in concentrated-coil or in wire-wound machines) the methodology has not been proved to give reliable results so far to the best of authors' knowledge.

An alternative method to compute end coil leakage inductances is the use of 3D FEA. This is known to be extremely heavy and time-consuming from a computational view-point and, in addition to this drawback, it suffers from the major problem of being little effective when applied to certain kinds of stator windings. An example is just given by the wire-wound machine used for validations in this paper: it can be seen from Fig. 14 how, in this case, end coils, after emerging from the stator stack, do not remain separated as in the case of pre-formed coils, but join together into a sort of single "bundle" which develops around the stator circumference. Inside this bundle, for obvious constructive reasons, end coils overlap and are partly twisted together in order to implement a dual-layer short-pitch distributed winding scheme. It is quite apparent that modeling such geometry for 3D FEA would be practically impossible, in addition to probably giving unreliable results

In conclusion, it is deemed that 3D FEA for end-coil leakage inductance computation, although beneficial in some cases, still poses serious computational challenges and may be even unfeasible for certain machine designs. For this reason, it appears that a leakage inductance computation method fully based on FEA (2D and 3D) could not be proposed for general validity.

VII. DISCUSSION

The subject matter presented in this paper may give rise to some points of discussion, regarding: its better practical applicability compared to alternative measurement techniques [18]-[21]; the possible extension of the method to electric machines with other number of phases (different from nine); the feasibility of a leakage inductance estimation procedure fully based on FEA simulations.

Regarding the former point, we can observe that the stator leakage inductance measurement methods used so far and based on tests with the rotor removed [18]-[21] can be applied to induction machines and not only to synchronous ones. On the other side, they need to be performed on the machine during manufacturing (i.e. before rotor mounting), while the proposed method can be applied to the built machine, based on measurements taken on such routine tests as the no-load and short circuit ones. It can be also objected that the proposed method, in addition to electrical measurements, requires some FEA. This, however, is normally required also for the measurements with the rotor removed to obtain sufficiently accurate results [19]-[21].

Regarding the possible extension of the method proposed in the paper to electric machines with a different number of phases, this is actually under investigation. In particular, when dealing with machines with a relatively low number of phases (such as five or six), the main challenge originates from the fact that space harmonics (which are responsible for the short circuit current distortion) can be included in the VSD model up to a limited harmonic order [2]. This makes the VSD model (Section II.B) little suitable and would make it necessary to work with the machine model in phase variables (Section II.A), so that the inductance identification procedure would not reduce to an algebraic problem as discussed in Section IV.

For machines with a high number of phases, on the other side, the same procedure described for the nine-phase case can be applied. However, some practical problems could arise in the accurate measurement of high-order harmonics (in the no-load voltage and short-circuit currents) which typically have very small amplitudes (as it can be seen in the nine-phase machine, too, for the ninth-order harmonics, Table V).

Finally, as regards the feasibility of a leakage inductance identification method fully based on FEA simulations, one should note that (as investigated in VI.C-1 and VI.C-2) a purely 2D FEA approach does not suffice as it cannot capture end coil leakage inductances, which can account for a significant portion of the overall leakage inductances. On the other side, the use of 3D FEA as a complementary tool to predict end coil leakage inductances, poses major challenges in terms of computational burden and appears very little suited for some winding designs, like that of the wire-wound machine used as a validation platform in this paper, as discussed in VI.C-3. As a consequence, some experimental data appear necessary, in general, to fully accomplish leakage inductance identification and the experimental data obtained from open-circuit and sustained short circuit tests, as proposed in this paper, are deemed the easiest useful experimental information to collect for the nine-phase machine case.

VIII. CONCLUSION

The accurate determination of stator leakage inductances of multiphase machines from either computation or measurements is a challenging task due to the complicated spatial distribution of leakage flux paths. Measurement methods have been proposed in the literature using properly calibrated FE models and electrical measurements performed on the wound stator before rotor mounting. In this paper, a new method is set forth to determine the stator self and mutual leakage inductances of a synchronous nine-phase machine based on two magneto-static analyses combined with measurements taken on the built machine during no-load and short-circuit routine tests. The magneto-static analyses are used to determine the magnetizing inductance matrix in the machine VSD model so that leakage inductances are left as the only unknown parameters in it. The harmonics detected in the no-load voltage and short circuit current waveforms are then used to identify such parameters through the numerical solution of a nonlinear algebraic system of equations. The proposed procedure has been experimentally applied and assessed on a nine-phase salient-pole wound-field machine comparing its results to the stator leakage inductances obtained from the conventional tests with the rotor removed. A satisfactory accordance has been found in the comparison. Further investigations are currently in progress to extend the proposed leakage inductance identification method to synchronous electric machines with a different number of phases.

REFERENCES

- [1] E. Levi, "Multiphase Electric Machines for Variable-Speed Applications", *IEEE Trans. on Ind. Electron.*, vol. 55, no. 5, pp. 1893-1909, May 2008.
- [2] E. Levi, R. Bojoi, F. Profumo, H.A. Toliyat, S. Williamson, "Multiphase induction motor drives - a technology status review", *IET Electric Power Applications*, no.4, pp.489-516, July 2007.
- [3] J.L.F. van der Veen, L.J.J. Offringa, and A.J.A. Vandenput, "Minimising rotor losses in high-speed high-power permanent magnet synchronous generators with rectifier loads", *Proc. Inst.*

Electr. Eng.—Electr. Power Appl., vol. 144, no. 5, pp. 1258–1266, Sep. 1997.

[4] J. Wang, R. Qu, and Y. Liu, “Comparison study of superconducting generators with multiphase armature windings for large-scale direct-drive wind turbines”, *IEEE Trans. Appl. Supercond.*, vol. 23, no. 3, article# 5201005, Jun. 2013.

[5] H.E. Jordan, R.C. Zowarka and S.B. Pratap, “Nine-Phase Armature Windings Design, Test, and Harmonic Analysis”, *IEEE Trans. on Magnetics*, vol. 41, no. 1, Jan. 2005, pp. 299-302.

[6] E. Jung, H. Yoo, S. Sul, H. Choi, and Y. Choi, “A nine-phase permanent magnet motor drive system for an ultrahigh-speed elevator”, *IEEE Trans. Ind. Appl.*, vol. 48, no. 3, pp. 987–995, May/June 2012.

[7] M. Ruba and D. Fodorean, “Analysis of fault-tolerant multiphase power converter for a nine-phase permanent magnet synchronous machine”, *IEEE Trans. Ind. Appl.*, vol. 48, no. 6, pp. 2092–2101, Nov./Dec. 2012.

[8] L. Parsa and T. Kim, “Reducing torque pulsation of multi-phase interior permanent magnet machines”, *41st IAS Annu. Meeting*, 2006, vol. 4, pp. 1978–1983.

[9] E. Levi, M. Jones, S. N. Vukosavic, and H. A. Toliyat, “Operating principles of a novel multiphase multimotor vector-controlled drive”. *IEEE Trans. Energy Convers.*, vol. 19, no. 3, pp. 508–517, Sep. 2004.

[10] P. Ponomarev, Y. Alexandrova, I. Petrov, P. Lindh, E. Lomonova, J. Pyrhonen, “Inductance Calculation of Tooth-Coil Permanent-Magnet Synchronous Machines”, *IEEE Transactions on Industrial Electronics*, vol. 61, no. 11, pp. 5966-5973, Nov. 2014.

[11] A. Tassarolo, C. Bassi, “Stator Harmonic Currents in VSI-Fed Synchronous Motors With Multiple Three-Phase Armature Windings”, *IEEE Transactions on Energy Conversion*, vol. 25, no. 4, pp. 974-982, Dec. 2010.

[12] D. Hadiouche, H. Razik, and A. Rezzoug, “On the modeling and design of dual-stator windings to minimize circulating harmonic currents for VSI-fed AC machines”, *IEEE Trans. Ind. Appl.*, vol. 40, no. 2, pp. 506–515, Mar./Apr. 2004.

[13] E. A. Klingshirn, “High phase order induction motors—Part I—Description and theoretical considerations”, *IEEE Trans. Power Appar. Syst.*, vol. PAS-102, no. 1, pp. 47–53, Jan. 1983.

[14] E. A. Klingshirn, “High phase order induction motors—Part II—Experimental results.” *IEEE Trans. Power Appar. Syst.*, vol. PAS-102, no. 1, pp. 54–59, Jan. 1983.

[15] S.D. Sudhoff, D.C. Aliprantis, B.T. Kuhn, P.L. Chapman, “Experimental characterization procedure for use with an advanced induction machine model”, *IEEE Transactions on Energy Conversion*, vol.18, no.1, pp.48.56, Mar 2003.

[16] D.C. Aliprantis, S.D. Sudhoff, B.T. Kuhn, “Experimental Characterization Procedure for a Synchronous Machine Model With Saturation and Arbitrary Rotor Network Representation”, *IEEE Transactions on Energy Conversion*, vol.20, no.3, pp.595-603, Sept. 2005.

[17] D.C. Aliprantis, S.D. Sudhoff, B.T. Kuhn, “A Synchronous Machine Model With Saturation and Arbitrary Rotor Network Representation”, *IEEE Transactions on Energy Conversion*, vol.20, no.3, pp.584-594, Sept. 2005.

[18] *Rotating Electrical Machines, Part 4: Methods for Determining Synchronous Machine Quantities from Tests*, IEC 34-4 Standard, 2008, pp. 22-24, 33-34, 52-53.

[19] D. Ban, D. Zarko, I. Mandic, “Turbogenerator end-winding leakage inductance calculation using a 3-D analytical approach based on the solution of Neumann Integrals”, *IEEE Transactions on Energy Conversion*, vol. 20, no. 1, pp.98-105, March 2005.

[20] A. Tassarolo, F. Luise, “An Analytical-Numeric Method for Stator End-Coil Leakage Inductance Computation in Multi-Phase Electric Machines”, *IEEE Industry Applications Society Annual Meeting 2008, IAS '08*, vol., no., pp.1.8, 5-9 Oct. 2008A.

[21] Tassarolo and D. Giulivo, “Analytical methods for the accurate computation of stator leakage inductances in multiphase synchronous machines”, *Int. Symp. Power Electron., Electr. Drives, Autom. Motion*, Pisa, Italy, Jun. 14–16, 2010, pp. 845–852.

[22] A. Tassarolo, “Accurate Computation of Multiphase Synchronous Machine Inductances Based on Winding Function Theory”, *IEEE Transactions on Energy Conversion*, vol.27, no.4, pp.895,904, Dec. 2012.

[23] A. Tassarolo, “On the modeling of poly-phase electric machines through Vector-Space Decomposition: Theoretical considerations”, *International Conference on Power Engineering, Energy and Electrical Drives, 2009. POWERENG '09*, pp.519-523, 18-20 March 2009.

[24] J. Figueroa, J. Cros, and P. Viarouge, “Generalized transformations for polyphase phase-modulation motors”, *IEEE Trans. Energy Convers.*, vol. 21, no. 2, pp. 332-341, Jun. 2006.

[25] L.A. Pereira, C.C. Scharlau, L.F.A. Pereira, J.F. Haffner, “General Model of a Five-Phase Induction Machine Allowing for Harmonics in the Air Gap Field,” *IEEE Transactions on Energy Conversion*, vol.21, no.4, pp.891,899, Dec. 2006.

[26] W. Winston, *Operations Research: Applications and Algorithms*, Wadsworth, 1994.

[27] M. Mezzarobba, L. Spangaro, A. Tassarolo, “Experimental evaluation of damper circuit influence on the performance of multiphase synchronous generators feeding multiple rectifiers”, *2011 International Conference on Power Engineering, Energy and Electrical Drives (POWERENG)*, 11-13 May 2011.



Alberto Tassarolo (M'06—SM'15) received his Laurea and Ph.D. Degrees in Electrical Engineering from the University of Trieste, Italy, in 2000 and from the University of Padova, Italy, in 2011, respectively. Until 2006, he worked in the design and development of innovative motors and generators for high power applications with NIDEC-ASI (formerly Ansaldo Sistemi Industriali). Presently, he is with the Engineering and Architecture Department of the University of Trieste, Italy, where he teaches the course of Electric

Machine Design. His main research interests are in the area of electric machine and drive modeling, design and analysis, a field in which he has authored more than 100 scientific papers. He acts as the principal investigator for various research projects in cooperation with leading electric machine manufacturers and final users, including the Italian Navy. He serves as an Editor for the IEEE TRANSACTIONS ON ENERGY CONVERSION and as an Associate Editor for the IEEE TRANSACTIONS ON INDUSTRY APPLICATIONS. He is a registered professional engineer in Italy.



Sobhan Mohamadian received his B.Sc. and M.Sc. degrees from Iran University of Science and Technology (IUST), Tehran, Iran, in 2007 and 2010, respectively, where he is currently pursuing the Ph.D. degree in Electrical Engineering. His research interests include power quality, power electronics and electrical machines. Between February 2014 and March 2015, he spent a period as a visiting scholar at the University of Trieste, Trieste, Italy, where he worked on research projects regarding high-power multiphase motor drives and multiphase machine modeling and analysis. Mr.

Mohamadian is a member of Iran's National Elite Foundation (INEF)



Mauro Bortolozzi received his Laurea degree with honors from the University of Trieste, Trieste, Italy, in 2012 and he is now working towards his Ph.D. degree in Electrical Engineering from the University of Trieste. His main research interests are in the field of electric machine design and optimization, with a special focus on high-efficiency electric motors and special alternators for distributed generation.

Mr. Bortolozzi is a registered professional engineer in Italy and is a member of AEIT — Italian Association of Electrical, Electronics, Automation, Information and Communication Technology.